THE JOURNAL OF PHYSICAL CHEMISTRY C

Article

pubs.acs.org/JPCC

Bisulfate Dehydration at Air/Solution Interfaces Probed by Vibrational Sum Frequency Generation Spectroscopy

Aaron M. Jubb and Heather C. Allen*

Department of Chemistry and Biochemistry, The Ohio State University, Columbus, Ohio 43210, United States

Supporting Information

ABSTRACT: The structure and organization of ions at vapor/solution interfaces have great implications for the reactivity and growth of atmospheric aerosols. Considering the ionic components of aqueous aerosols, sulfate species are one of the most prevalent due to high levels of $SO_{2(g)}$ emission to the atmosphere from biofuel burning and volcanic eruptions. Atmospheric $SO_{2(g)}$ can undergo direct gas phase oxidation or experience dissolution and subsequent oxidation to sulfate species within aqueous aerosols, where, depending on the pH level, sulfate may exist as SO_4^{2-}, HSO_4^-, or H_2SO_4. Here we probe the molecular environment experienced by the bisulfate anion (HSO_4^-) at vapor/solution interfaces for H_2SO_4, Na_2SO_4, and $MgSO_4$ solutions via vibrational sum frequency generation (VSFG) spectroscopy. VSFG is an inherently interface specific nonlinear optical spectroscopy and is a powerful tool for the study of interfacial structure and organization. Our VSFG results are compared to bisulfate behavior in bulk aqueous solution observed using Raman and infrared spectroscopies. The presence of Na^+ and Mg^{2+} is observed to perturb HSO_4^- anion hydration compared to H^+ which manifests as a blue shift in the observed SO_3 symmetric stretching mode frequency of HSO_4^-. This perturbation is greatly exaggerated for interfacial HSO_4^- anions residing within vapor/solution interfaces relative to bulk solution. Mg^{2+} ions are found to disrupt the net bisulfate population hydration within the vapor/solution interfaces tested, while Na^+ ions only influence a subpopulation of the interfacial bisulfate distribution. This difference is attributed to the much greater propensity for aqueous solvation that Mg^{2+} exhibits compared to Na^+. Our results are interpreted with a perspective toward understanding interfacial acid dissociation for the bisulfate anion and the role that this may play for tropospheric acidic aerosols.

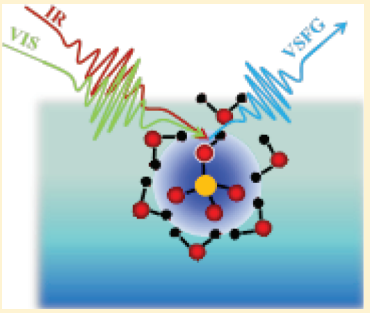

INTRODUCTION

The structure and reactivity of simple inorganic ions at vapor/solution interfaces has been an intense area of study the past decade[1−12] following the pioneering work of Jungwirth and Tobias,[13] who challenged the long-held belief that ions are depleted from vapor/solution interfaces based on surface tension measurements.[14,15] Ion behavior at vapor/solution interfaces has important implications for atmospheric aerosols as the interface between the gas phase atmosphere and the liquid phase aerosol plays host to reactions which control the growth and uptake of the aerosol.[4,16−19] Aerosol reactivity and growth are vital to understand as the climate forcing effects of aerosols on Earth's total albedo is poorly understood today.[20]

Sulfate (SO_4^{2-}) is a major ionic component of tropospheric aerosols, which may exist as SO_4^{2-}, bisulfate (HSO_4^-), or molecular sulfuric acid (H_2SO_4) depending on solution pH. High aerosol SO_4^{2-} content is mainly due to $SO_{2(g)}$ uptake and subsequent oxidation within the solution phase of aqueous aerosols.[11,16−19,21] Sulfate species (SO_4^{2-}, HSO_4^-, H_2SO_4, and organosulfates) are also very prevalent in marine aerosols due to sulfate being the third most abundant ionic species in seawater by weight and the large atmospheric release of sulfur compounds from algal metabolic processes.[17,19,22−25] Aerosol sulfate content is directly related to the growth potential of the associated aerosol due to sulfate ion's large propensity for hydration.[4,26−28] Sulfate content and acidity of aqueous aerosols has also been linked to important atmospheric processes such as catalytic production of chlorine radical and secondary organic aerosol formation.[18,29−31]

Despite the relative importance in understanding interfacial processes to explain the physical and chemical phenomena that aqueous aerosols partake in, the vapor/solution interface remains very difficult to experimentally probe. The application of optical nonlinear spectroscopies such as second harmonic generation (SHG) and vibrational sum frequency generation (VSFG) spectroscopies, which are inherently interface specific, along with accompanying theoretical studies, have provided insight into the underlying driving forces for many interfacial processes.[1−5,9,32−44] Generally these studies have focused on the elucidation of interfacial water structure as a probe of the molecular environment at the vapor/solution interface.[1,3,7,9−11,32,33,38,39,43−50] However, there have been several recent studies demonstrating the suitability of SHG and VSFG to directly interrogate interfacial ions.[34,35,37,51−54]

In a recent series of papers, Morita and co-workers have revealed the power of combining the VSFG method with theoretical modeling to probe acid dissociation within the vapor/solution interface for a series of H_2SO_4 solutions with a perspective toward tropospheric acidic aerosols.[34,53,54] These

Received: March 17, 2012
Published: May 22, 2012

   dx.doi.org/10.1021/jp302585h | J. Phys. Chem. C 2012, 116, 13161−13168

studies investigate both the interfacial water structure and the sulfate species' vibrational modes at vapor/solution interfaces. Their findings indicate that the first acid dissociation of H_2SO_4 (eq 1) in vapor/solution interfaces is bulklike for both concentrated and dilute solutions but that the second acid dissociation (eq 2) is suppressed for high concentrations, $[H_2SO_4] > 0.2$ mole fraction (x), within the interface.[34,53,54]

$$H_2SO_4 + H_2O \leftrightarrow H_3O^+ + HSO_4^- \qquad pK_{a1} \ll 0 \tag{1}$$

$$HSO_4^- + H_2O \leftrightarrow H_3O^+ + SO_4^{2-} \qquad pK_{a2} = 2 \tag{2}$$

While these studies provide critical insight into the behavior of sulfate species at vapor/solution interfaces, they do not address the role that cation identity may play for the interfacial behavior of sulfate species, such as HSO_4^-.

Here we report on the effect that cation (Na^+ or Mg^{2+}) identity has on HSO_4^- anions within vapor/solution interfaces probed via conventional VSFG spectroscopy. H_2SO_4 solutions were studied as a comparison to the findings of Morita and co-workers[34,53,54] as well as providing a basis from which to judge cation effects on bisulfate's molecular environment. Na^+ and Mg^{2+} cations were chosen as they represent the most prevalent cation species within seawater by weight and thus should be the most prevalent cations in marine aqueous aerosols.[22,23] Our VSFG findings show that both Na^+ and Mg^{2+} cations perturb the hydration of interfacial HSO_4^-, analogous to a dehydration effect, with the Mg^{2+} ions exhibiting a larger influence than Na^+. These VSFG findings are compared to bulk solution studies on HSO_4^- behavior completed using conventional Raman and infrared spectroscopies.

EXPERIMENTAL METHODS

VSFG spectroscopy is a nonlinear optical spectroscopy based on the detection of coherent light generated by the second-order induced polarization of molecules subjected to incident high intensity electric fields.[55] The detected VSFG signal intensity, I_{VSFG}, is proportional to the square modulus of the effective second-order nonlinear susceptibility, $\chi^{(2)}_{eff}$, as well as the intensity of the two input beams, I_{Vis} and I_{IR} (eq 3). The

$$I_{VSFG} \propto |\chi^{(2)}_{eff}|^2 I_{Vis} I_{IR} \tag{3}$$

effective second-order nonlinear susceptibility is proportional to the molecular hyperpolarizability, β_{lmn} (eq 4), which demonstrates the dependence of VSFG activity on the Raman, $\langle g|\alpha_{lm}|\nu\rangle$, and infrared, $\langle \nu|\mu_n|g\rangle$, transitions for the molecular vibration of interest. This dependence gives rise to the VSFG selection rule which states that a molecular vibration must be both Raman and infrared active to be VSFG active.[3]

$$\chi^{(2)}_{eff} \propto \beta_{lmn} = \frac{\langle g|\alpha_{lm}|\nu\rangle\langle \nu|\mu_n|g\rangle}{\omega_{IR} - \omega_\nu + i\Gamma_\nu} \tag{4}$$

Details of the VSFG spectrometer used for this study have been previously published.[51] Briefly, the fundamental output (1064 nm) from an Nd:YAG laser (26 ps pulse duration, 20 Hz repetition rate, EKSPLA, PL2143A/20/SS) is frequency-doubled (second harmonic) to produce a fixed frequency visible beam (532.1 nm) and used to pump an optical parametric generator (OPG) (EKSPLA, PG401/DFG2-16P) which produces tunable infrared light (8−12 μm) via difference frequency mixing within a GaSe crystal. The visible and infrared beams were overlapped spatially and temporally on the sample surface at an $x-y-z$ sample stage with input angles of 60 and 55°, respectively, relative to the surface normal of the sample solution. Intensities of the input beams at the sample stage were generally 300 μJ/pulse for the visible beam and 50 μJ/pulse for the infrared beam. The energy profiles of the input visible and infrared beams were monitored in real time during spectral acquisition, and all VSFG spectra have been normalized to these profiles to remove shot-to-shot noise. All VSFG spectra were collected using the SSP polarization combination, where the letter refers to the polarization state of each beam in decreasing order of frequency (VSFG, visible, infrared). The generated VSFG beam was collected in the reflection geometry and sent to an electron multiplying charge-coupled device (EMCCD) (Andor Technology, Newton, DU97ON-BV) for detection. The resolution of the collected VSFG spectra is 6 cm^{-1} full width at half-maximum (fwhm). All spectra were collected with 30 s acquisition times per infrared wavelength with 150× electron multiplying gain. All VSFG spectra shown are the average of three to four spectra. The VSFG spectra have been calibrated against the SO_3 symmetric stretching peak at 1070 cm^{-1} of a sodium dodecyl sulfate (SDS) monolayer on neat water collected with VSFG at the beginning of each day experiments were run.[56]

All Raman spectra were collected using 200 mW output from a 785 nm continuous wave diode laser (Process Instruments, ECL-785-300-SH) coupled to a fiber optic probe (InPhotonics, RPS785/12-5) equipped with a 7 mm focal lens. The fiber optic probe was also used to collect the generated Raman Stokes scatter in the 0° direction before the collected signal was sent to a monochromator (Princeton, Pixis 400) equipped with a thermoelectrically cooled CCD (Princeton, Acton LS785), calibrated versus the output of a Hg lamp and the Raman spectrum of crystalline naphthalene (Sigma Aldrich, > 99% pure), for detection. The Raman spectra are the sum of a 30 s acquisition. The infrared spectra shown were all taken using a home-built attenuated total reflection (ATR) apparatus equipped with a 45° cut ZnSe element to achieve total internal reflection of the infrared beam. This apparatus was mounted in a conventional bench-top Fourier transform (FT) infrared spectrometer (Spectrum 100, Perkin-Elmer). The infrared spectra shown are the average of 100 scans normalized against a background spectrum of pH 1 water (0.1 M HCl) for the salt solutions and the bare ATR element spectrum for the H_2SO_4 solutions.

All salt solutions were prepared by mixing the appropriate amount of salt, Na_2SO_4 (99+% pure, Acros Organics, crystalline, anhydrous) or $MgSO_4$ (>99.5% pure, Fisher, powder, anhydrous), with nanopure water (18.3 MΩ, Nano-Pure, Barnstead/Thermolyne). For pH 1 salt solutions the salt solution was prepared and then brought to the appropriate pH using concentrated HCl (37 wt %, Fisher, trace metal grade). The presence of Cl^- in the solutions is not predicted to substantially affect our results. H_2SO_4 solutions were prepared by mixing concentrated H_2SO_4 (Fisher, Certified ACS Plus) with nanopure water to the desired concentration. SDS solutions were prepared using solid SDS powder (99+% pure, ACS reagent grade, Sigma-Aldrich) and nanopure water.

RESULTS AND DISCUSSION

Figure 1 presents three VSFG spectra showing the SO_3 symmetric stretching mode (ν_{SS}-SO_3) of interfacial HSO_4^-

dx.doi.org/10.1021/jp302585h | J. Phys. Chem. C 2012, 116, 13161−13168

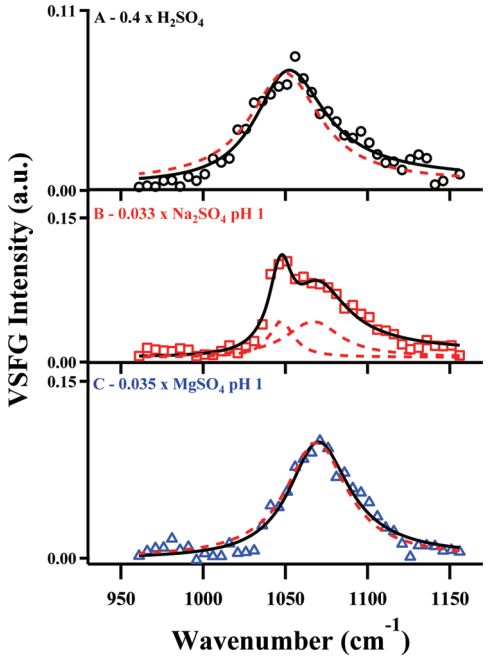

Figure 1. SSP VSFG spectra from (A) 0.4*x* H_2SO_4, (B) pH 1 0.033*x* Na_2SO_4, and (C) pH 1 0.035*x* $MgSO_4$ solutions. Data (symbols), fits to modified Lorentzian profile (solid black lines), and Lorentzian peak components (dashed red lines) are shown.

anions for a 0.4*x* H_2SO_4 solution (Figure 1A) and pH 1 solutions of 0.033*x* Na_2SO_4 (Figure 1B) and 0.035*x* $MgSO_4$ (Figure 1C). For the salt solutions, as the solution pH drops below 2, the protonation of SO_4^{2-} becomes favorable (eq 2) and HSO_4^- is formed in solution. The 0.4*x* H_2SO_4 VSFG spectrum is in good agreement with published literature results from Miyamae et al.[53] A concentration of 0.4*x* H_2SO_4 was chosen as, at this concentration, the predominant ionic species in sulfuric acid solutions is HSO_4^- maximizing the VSFG signal arising from interfacial HSO_4^- anions.[53] Approximately 0.03*x* was chosen as the representative salt solution concentration, analogous to ~2 M, as this concentration approaches the aqueous solubility limit of Na_2SO_4 and the VSFG intensity was much weaker for more dilute salt concentrations tested.[23] As high salt concentrations can be found in aqueous tropospheric aerosols, the concentration regime of 0.03*x* seems to be a reasonable one to use for this study.[17,19,45,57,58] The ν_{SS}-SO_3 VSFG signal intensity for both Na_2SO_4 (Figure 1B) and $MgSO_4$ (Figure 1C) solutions at pH 1 is comparable to the 0.4*x* H_2SO_4 solution results (Figure 1A). While the ν_{SS}-SO_3 VSFG signal intensity is comparable among all solutions tested, the ν_{SS}-SO_3 peak frequency varies between solutions. The Na_2SO_4 and $MgSO_4$ solutions exhibit blue-shifted components for the ν_{SS}-SO_3 peak relative to the ν_{SS}-SO_3 peak position of the 0.4*x* H_2SO_4 solution, indicating perturbation to the HSO_4^- interfacial environment.

For Na_2SO_4 and $MgSO_4$ both neutral, pH 7, and acidic, pH 1, solutions were tested using VSFG. It was not possible to resolve any spectral features in the S−O stretching region from 980 to 1170 cm^{-1} for the neutral solutions (see the Supporting Information for spectra). The absence of any VSFG signal for the neutral salt solutions does not indicate an absence of SO_4^{2-} within the vapor/solution interface for these solutions. The lack of any appreciable SO_4^{2-} signal for the pH 7 salt solutions is most likely due to a confluence of two factors, including the preference of SO_4^{2-} to reside near the bottom of the vapor/solution interface and the low molecular hyperpolarizability of tetrahedral SO_4^{2-} molecular vibrations (eq 4).[4,6,34,46,47,53,54] Regardless, these factors render the direct interrogation of SO_4^{2-} vibrational modes within the vapor/solution interface infeasible using a VSFG spectroscopic approach. In contrast, the HSO_4^- vibrational modes are strongly Raman and infrared active and HSO_4^- has been shown to have increased surface preference versus SO_4^{2-}, most likely due to its decreased valency.[34,54] The HSO_4^- anion possesses C_s symmetry but effectively behaves with C_{3v} symmetry, which has been demonstrated in many Raman, infrared, and theoretical studies.[59−64] The effective C_{3v} symmetry of HSO_4^- results in the strong molecular hyperpolarizability for the ν_{SS}-SO_3 mode, enabling the direct interrogation of HSO_4^- anions within vapor/solution interfaces.

It is clear from Figure 1 that the presence of either Na^+ or Mg^{2+} cations within the vapor/solution interfaces tested results in a blue shift for the observed HSO_4^- ν_{SS}-SO_3 peak frequency. The spectra in Figure 1 have all been fit using a modified Lorentzian profile, where the solid black lines correspond to the total fit and the dashed red lines are the corresponding Lorentzian peak components (see the Supporting Information for the VSFG fitting profile). Both the H_2SO_4 and $MgSO_4$ solutions are best fit with one Lorentzian component, centered at 1050 and 1069 cm^{-1}, respectively. The Na_2SO_4 solution features a bimodal distribution with two Lorentzian component peaks centered at 1048 and 1067 cm^{-1}, suggesting that there are two distinct populations of HSO_4^- at vapor/solution interfaces for pH 1 Na_2SO_4 solutions. The VSFG fitting results for all solutions have been summarized in Table 1.

The VSFG results (Figure 1) can be interpreted by considering the effects that cation−anion interaction can have on anion vibrational modes. One type of cation−anion interaction is the formation of solution ion pairs. Ion pair formation within salt solutions has been the subject of intense experimental and theoretical study for decades as the speciation of ionic solutions has large implications for many areas of physical and biological sciences.[26,28,45,51,52,57,58,62,63,65−88] Vibrational spectroscopic techniques such as Raman and infrared have been successfully applied to study ion pairing effects between SO_4^{2-} and Na^+ or Mg^{2+} in bulk solution by a number of groups.[28,57,66−70,79,83−87] It is generally accepted that both Na^+ and Mg^{2+} form ion pairs with SO_4^{2-} in bulk solution[79,85]

Table 1. Curve-Fitting Results for VSFG Spectra

		nonresonant terms		peak 1			peak 2		
	concn	B	ϕ	ω_ν (cm^{-1})	A_ν	Γ (cm^{-1})	ω_ν (cm^{-1})	A_ν	Γ (cm^{-1})
H_2SO_4	0.4*x*	0.03	0.01	1050	6.9	26.0	N/A	N/A	N/A
Na_2SO_4	0.033*x*	0.05	0.03	1048	1.7	8.6	1067	3.8	19.7
$MgSO_4$	0.035*x*	0.02	0.00	N/A	N/A	N/A	1069	7.0	22.4

dx.doi.org/10.1021/jp302585h | J. Phys. Chem. C 2012, 116, 13161−13168

following the stepwise association mechanism first proposed by Eigen and Tamm.[65]

Ion pairing involving SO_4^{2-} manifests in Raman spectra as a small shoulder on the blue side of the ν_{SS}-SO_4^{2-} peak centered at 980 cm^{-1}; with increased temperature or decreasing water content this small shoulder grows into a distinct peak centered at 993 cm^{-1}.[79,85−87] The ν_{SS}-SO_4^{2-} blue shift observed for ion pairs involving SO_4^{2-} is most likely due to the symmetry lowering experienced by the SO_4^{2-} tetrahedron on ion pair formation. This relationship between symmetry lowering and a blue shift for the ν_{SS}-SO_4^{2-} peak frequency is also observed in Raman spectra of solid sulfate salts.[86,89] However, an observed blue shift for anion vibrational modes, as observed for bulk aqueous SO_4^{2-} ion pair complexes, does not always indicate ion pair formation. For example, with ion pair formation involving nitrate (NO_3^-) anions, a distinct red shift for the NO_3^- symmetric stretching vibrational mode is observed with Raman spectroscopy.[51,82] While there are fewer studies investigating the ion pair formation with aqueous HSO_4^- compared to SO_4^{2-}, a distinct red shift for the ν_{SS}-SO_3 peak of HSO_4^- has also been observed with ion pair formation by Fung and Tang[71] using Raman spectroscopy in a study of supersaturated droplets of $(NH_4)HSO_4$, $NaHSO_4$, and $KHSO_4$. This trend is similar to the red shift observed for ion pairs involving nitrate in the NO_3^- symmetric stretch vibrations.

From the results of Fung and Tang[71] it becomes necessary to consider effects that cation interactions may have on interfacial HSO_4^- other than ion pair formation in order to rationalize the observed ν_{SS}-SO_3 peak blue shifts for the two salt solutions. By considering effects of hydration on the HSO_4^- ν_{SS}-SO_3 peak frequency, clear interpretation of the VSFG results presented in Figure 1 is possible. Hydrogen bonding between waters of solvation and the aqueous HSO_4^- anion effectively lengthen the S═O bonds of HSO_4^- by abstracting electron density from the bond.[64] When these solvating hydrogen bonds are weakened, this abstraction is reduced and the S═O bond is strengthened resulting in a blue shift of the ν_{SS}-SO_3 peak frequency; this effect has been directly observed by Walrafen et al. for H_2SO_4 solutions with increased temperature.[64] Dehydrating effects have also been invoked to explain blue shifts for NO_3^- vibrational mode frequency in studies of NO_3^- speciation within aqueous solutions,[51,80,82] as well as the symmetric P−O stretching mode of phosphate headgroup moieties with film compression for Langmuir monolayers of the phospholipid dipalmitoyl phosphatidylcholine.[90]

Considering the VSFG results in Figure 1, it can be surmised that the presence of Na^+ and Mg^{2+} within the vapor/solution interface perturbs interfacial HSO_4^- hydration. This results in the observed blue shift of the VSFG ν_{SS}-SO_3 peak frequency for the salt solutions. There is no evidence of ion pair formation between HSO_4^- and Na^+ or Mg^{2+} as this is predicted to result in a red shift for the ν_{SS}-SO_3 peak. That the presence of cations within the vapor/solution would affect the hydration of interfacial HSO_4^- is an intuitive result with the relatively high concentration of ions in the solutions tested. However, that Mg^{2+} would perturb HSO_4^- hydration to a greater degree than Na^+ is nonintuitive considering the relative surface preference and higher number density (∼2 times) of Na^+ compared to Mg^{2+}.[58] This result can be interpreted from the high affinity for solvating water that Mg^{2+} exhibits compared to Na^+ due to the high charge density of the Mg^{2+} ion.[45,58,76,85,91] Mg^{2+} affinity for solvating water makes it highly disruptive to the hydrogen bonding of other interfacial ion solvation spheres.

Due to the strong solvation properties of Mg^{2+}, bisulfate anion hydration is highly perturbed by the presence of Mg^{2+} within the interface. This results in the observed blue shift for the ν_{SS}-SO_3 peak of 19 cm^{-1} versus the peak position for H_2SO_4. In contrast, Na^+ only affects a subpopulation of the bisulfate distribution within the interface, most likely due to the generally weak hydration properties of Na^+, resulting in the bimodal distribution observed for the ν_{SS}-SO_3 peak in Figure 1B.[91] It is also observed in Figure 1B that the bandwidth of the lower frequency peak component is approximately half that of the higher frequency peak component. The origin of this decreased bandwidth is unclear; but the result of interference effects arising from the near-by higher frequency component can be neglected as the origin for this spectral feature as fitting the two peak components with opposite phases did not affect the bandwidth of the lower frequency peak component. The excitation lifetimes for the ν_{SS}-SO_3 modes of unperturbed and perturbed HSO_4^- may vary and this could be the source of the observed bandwidth discrepancies.

Recent cluster studies by Yacovitch et al. on bisulfate which indicate that the ν_{SS}-SO_3 peak frequency of HSO_4^- is not sensitive to hydration should be considered.[92] Yacovitch et al. examined aqueous HSO_4^- clusters with up to n = 16 water molecules and found that the ν_{SS}-SO_3 peak frequency was constant at 1049 cm^{-1} for all cluster sizes. While this frequency is in excellent agreement with our VSFG results for a 0.4x H_2SO_4 solution (Figure 1A), it is substantially higher than the value of ∼1035 cm^{-1} observed for bulk aqueous HSO_4^- solutions with infrared spectroscopy, both in the current study and elsewhere.[60] The consistency for the ν_{SS}-SO_3 peak frequency with increasing cluster size observed by Yacovitch et al.[92] may reflect the interfacial nature, which is inherently disruptive to hydrogen bonding, even for the largest clusters tested (n = 16).

The response of HSO_4^- to the presence of cations in bulk solutions exhibits trends similar to those observed for vapor/solution interfaces, but to a lesser degree. Shown in Figures 2−4 are bulk solution Raman and infrared spectra for a H_2SO_4 solution, and pH 1 solutions of Na_2SO_4 and $MgSO_4$, respectively. It is clear from Figure 2, corresponding to bulk solution spectra from a 0.4x H_2SO_4 solution, that Raman spectra originating from solutions where both HSO_4^- and SO_4^{2-} exist are generally much easier to unambiguously interpret compared to infrared spectra of the same solution. This is due to the strong infrared activity of broad, overlapping asymmetric stretching vibrations from SO_4^{2-} and HSO_4^- anions. Thus, while the infrared spectra for all solutions tested are shown for completeness, only the Raman spectra are considered when discussing cation effects on bulk HSO_4^- solution behavior.

Figures 3 and 4 are the Raman and infrared spectra for pH 1 0.009x, 0.017x, and ∼0.034x solutions of Na_2SO_4 and $MgSO_4$, respectively. These spectra exhibit both SO_4^{2-} and HSO_4^- signatures, but the SO_4^{2-} signatures dominate the spectra. This is because, at pH 1, the solution concentration of HSO_4^- is only ∼0.0017 x (0.1 M) due to the limiting amount of H^+ present in solution. This result reinforces the idea that HSO_4^- exhibits slight surface preference since HSO_4^- features are clearly observable in the salt solution VSFG spectra (Figure 1), even for this concentration of HSO_4^-. Examining the ν_{SS}-SO_3 region in the Raman spectra for the two bulk salt solution series (Figure 5), it is evident that the pH 1 Na_2SO_4 solutions exhibit greater ν_{SS}-SO_3 intensity than the pH 1 $MgSO_4$ spectra. This

dx.doi.org/10.1021/jp302585h | J. Phys. Chem. C 2012, 116, 13161−13168

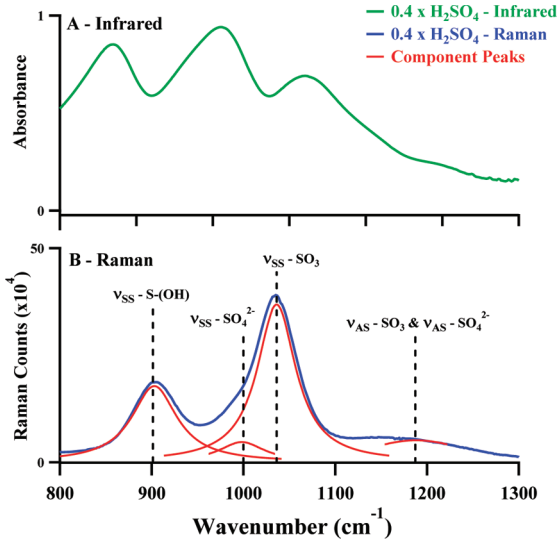

Figure 2. Infrared (A) and Raman (B) spectra from a 0.4*x* H_2SO_4 solution. Data (infrared, green solid line; Raman, blue solid line) and Lorentzian peak components of Raman fit (red solid lines) are shown. Spectral assignments, indicated by dashed vertical lines, are given for the Raman spectrum (B) but not included for infrared spectrum (A) due to overlapping peaks in infrared spectrum.

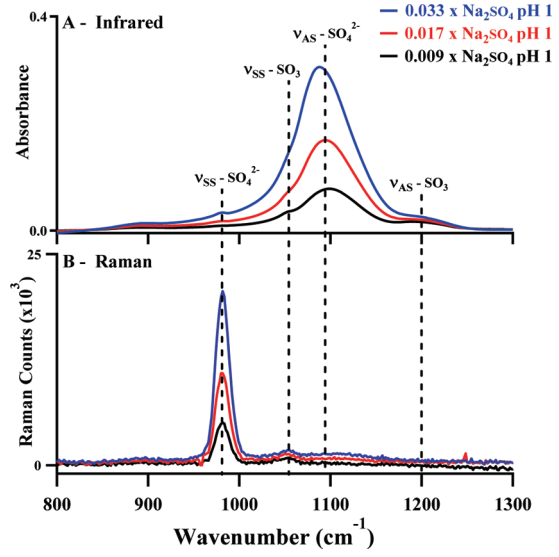

Figure 3. Infrared (A) and Raman (B) spectra from a pH 1 Na_2SO_4 solution series. Legend applies to both spectra sets. Spectral assignments given for both infrared (A) and Raman (B) spectra, indicated with dashed vertical lines. Weak ν_{SS}-SO_3 peak at ~1050 cm^{-1} in infrared spectra (A) is difficult to distinguish due to the broad, strongly absorbing ν_{AS}-SO_4^{2-} peak of sulfate at ~1100 cm^{-1}.

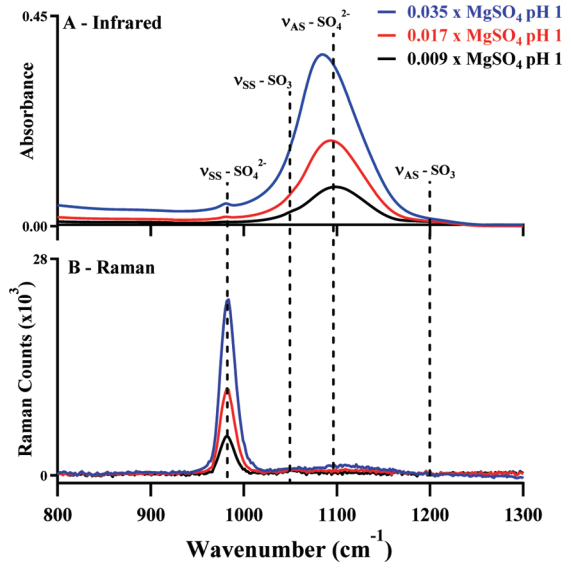

Figure 4. Infrared (A) and Raman (B) spectra from a pH 1 $MgSO_4$ solution series. Legend applies to both spectra sets. Spectral assignments given for both infrared (A) and Raman (B) spectra, indicated with dashed vertical lines. ν_{SS}-SO_3 peak at ~1050 cm^{-1} in (A) and (B) is more difficult to distinguish compared to Na_2SO_4 results (Figure 3).

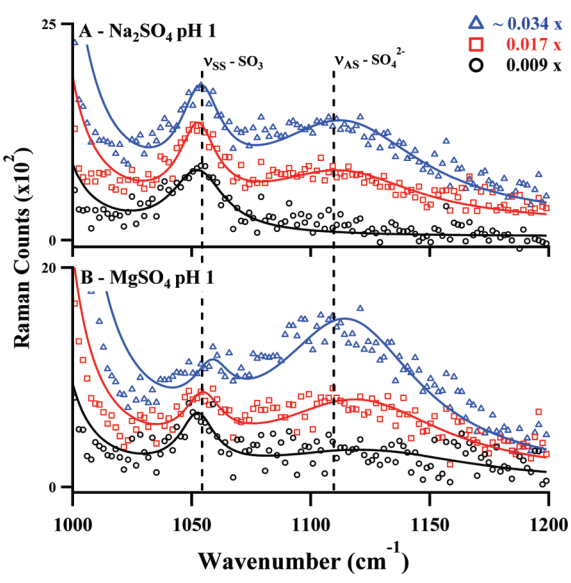

Figure 5. Raman spectra zoom in on the ν_{SS}-SO_3 peak region for pH 1 Na_2SO_4 (A) and $MgSO_4$ (B) solution series. Data (symbols) and Lorentzian fits to data (solid lines) shown. Legend applies to spectra in both (A) and (B), where ~0.034*x* (blue triangles), 0.017*x* (red squares), and 0.009*x* solutions (black circles) are indicated. Spectral assignments are given, indicated with dashed vertical lines. Spectra are offset for clarity.

phenomenon was first observed in 1972 by Daly et al. and was interpreted as an indication of increased ion association within $MgSO_4$ solutions versus Na_2SO_4 solutions.[69] The increased ion pair formation between Mg^{2+} and SO_4^{2-} seems to effectively inhibit the protonation of SO_4^{2-} to HSO_4^- in solution. While this is an interesting result it does not affect the interpretation of our results and, as such, will not be discussed further.

By fitting the bulk solution Raman spectra (Figures 2 −4), it is possible to examine the impact that increased solution concentration and cation identity have on ν_{SS}-SO_3 peak frequency for bulk HSO_4^- solutions (see the Supporting Information for complete fitting results). Figure 6 plots the ν_{SS}-SO_3 peak frequency with one standard deviation indicated for the bulk solution Raman spectra as well as the VSFG results versus the respective solution concentration. It is clear that the ν_{SS}-SO_3 peak frequency increases in bulk solution with increased solution concentration and with cation identity as $H^+ < Na^+ < Mg^{2+}$. Interestingly, the degree of blue shift observed for the ν_{SS}-SO_3 peak frequency between the bulk solution and interface results is very similar to the observed

dx.doi.org/10.1021/jp302585h | J. Phys. Chem. C 2012, 116, 13161−13168

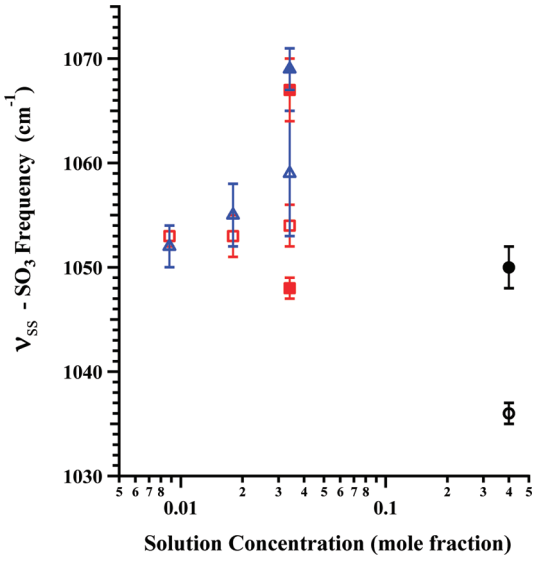

Figure 6. Peak frequency for ν_{SS}-SO_3 mode versus solution concentration in mole fraction for VSFG (solid symbols) and Raman (open symbols) results. H_2SO_4 solution results (black circles), Na_2SO_4 solution results (red squares), and $MgSO_4$ solution results (blue triangles) are shown. Error bars indicate one standard deviation from ν_{SS}-SO_3 spectral fits.

degree of blue shift in the presence of Na^+ or Mg^{2+} ions within the data sets. Thus, HSO_4^- ions at vapor/salt-solution interfaces should exhibit the highest ν_{SS}-SO_3 peak frequency, and indeed this is observed in our VSFG results for pH 1 Na_2SO_4 and $MgSO_4$ solutions. These results suggest that the presence of cations within bulk solution is just as disruptive to HSO_4^- hydration as is residing within a vapor/solution interface free of cations, which is an inherently dehydrating environment relative to the bulk.

CONCLUSIONS

The behavior of HSO_4^- at vapor/solution interfaces for H_2SO_4, Na_2SO_4, and $MgSO_4$ solutions was examined as a function of cation identity via VSFG spectroscopy. The ν_{SS}-SO_3 vibrational mode of the HSO_4^- anion provides an excellent probe of the molecular environment experienced by HSO_4^- within vapor/solution interfaces. The presence of Na^+ and Mg^{2+} is found to perturb the hydration of HSO_4^- anions, resulting in an observed blue shift for the ν_{SS}-SO_3 peak frequency. Mg^{2+} is found to perturb the entire population of interfacial HSO_4^- due to its strong solvation properties while Na^+ is less disruptive, resulting in a bimodal distribution for the ν_{SS}-SO_3 peak in the VSFG spectrum.[58,91] These results are rationalized by considering the effect that dehydration, or hydrogen bond disruption, has on the HSO_4^- ν_{SS}-SO_3 mode, which is to shorten the S═O bond length resulting in a higher frequency of vibration.[58,64,82] No ion pair formation is detected between interfacial HSO_4^- anions and Na^+ or Mg^{2+} cations. The bulk solution results from Raman spectroscopy reflect trends similar to those of the interface but with the observed ν_{SS}-SO_3 peak frequency blue shifting to a lesser degree than what is observed with VSFG for interfacial HSO_4^-. Infrared spectroscopic results do not offer any clear indication of bulk bisulfate behavior due to the HSO_4^- ν_{SS}-SO_3 mode being obscured by the broad, strong SO_4^{2-} asymmetric stretching modes in the infrared spectra.

These results may have implications for tropospheric aqueous sulfate containing aerosols. In acidic aerosols, which may feature Na^+ or Mg^{2+} cations along with HSO_4^- anions within the aerosol vapor/liquid interface, our results indicate that the HSO_4^- anions will feel some degree of cation induced disruption to their hydration structure. This perturbation to HSO_4^- hydration may retard the acid dissociation of HSO_4^- beyond what is predicted for H_2SO_4 solutions at vapor/solution interfaces.[34,53,54] By perturbing interfacial HSO_4^- dissociation to H^+, known to prefer the topmost layer of vapor/solution interfaces,[36] and SO_4^{2-}, which will preferentially segregate to the interior of the aerosol,[46,47] cations residing in the vapor/solution interface may inhibit important acid catalyzed aerosol processes such as secondary organic aerosol formation.

ASSOCIATED CONTENT

Supporting Information

VSFG spectra of pH 7 Na_2SO_4 and $MgSO_4$ solutions, modified Lorentzian profile used to fit VSFG spectra, representative Raman spectrum fit, and fitting parameters and results for ν_{SS}-SO_3 peak from Raman spectral fits. This material is available free of charge via the Internet at http://pubs.acs.org.

AUTHOR INFORMATION

Corresponding Author

*E-mail: allen@chemistry.ohio-state.edu.

Notes

The authors declare no competing financial interest.

ACKNOWLEDGMENTS

We gratefully acknowledge NSF-CHE (Grant 0749807) and DOE-BES Geochemistry (Grant DE-FG02-04ER15495) for funding this work.

REFERENCES

(1) Gopalakrishnan, S.; Liu, D. F.; Allen, H. C.; Kuo, M.; Shultz, M. J. *Chem. Rev.* **2006**, *106*, 1155−1175.
(2) Geiger, F. M. *Annu. Rev. Phys. Chem.* **2009**, *60*, 61−83.
(3) Jubb, A. M.; Hua, W.; Allen, H. C. *Annu. Rev. Phys. Chem.* **2012**, *63*, 107−130.
(4) Jungwirth, P.; Tobias, D. J. *Chem. Rev.* **2006**, *106*, 1259−1281.
(5) Jungwirth, P.; Winter, B. *Annu. Rev. Phys. Chem.* **2008**, *59*, 343−366.
(6) Petersen, P. B.; Saykally, R. J. *Annu. Rev. Phys. Chem.* **2006**, *57*, 333−364.
(7) Schnitzer, C.; Baldelli, S.; Shultz, M. J. *J. Phys. Chem. B* **2000**, *104*, 585−590.
(8) Zhang, Y. J.; Cremer, P. S. *Annu. Rev. Phys. Chem.* **2010**, *61*, 63−83.
(9) Raduge, C.; Pflumio, V.; Shen, Y. R. *Chem. Phys. Lett.* **1997**, *274*, 140−144.
(10) Baldelli, S.; Schnitzer, C.; Shultz, M. J. *J. Phys. Chem. B* **1997**, *101*, 10435−10441.
(11) Tarbuck, T. L.; Richmond, G. L. *J. Am. Chem. Soc.* **2006**, *128*, 3256−3267.
(12) Ghosal, S.; Hemminger, J. C.; Bluhm, H.; Mun, B. S.; Hebenstreit, E. L. D.; Ketteler, G.; Ogletree, D. F.; Requejo, F. G.; Salmeron, M. *Science* **2005**, *307*, 563−566.
(13) Jungwirth, P.; Tobias, D. J. *J. Phys. Chem. B* **2001**, *105*, 10468−10472.
(14) Heydweiller, A. *Ann. Phys.* **1910**, *33*, 145−148.
(15) Onsager, L.; Samaras, N. N. T. *J. Chem. Phys.* **1934**, *2*, 528.
(16) Charlson, R. J.; Schwartz, S. E.; Hales, J. M.; Cess, R. D.; Coakley, J. A.; Hansen, J. E.; Hofmann, D. J. *Science* **1992**, *255*, 423−430.

(17) Finlayson-Pitts, B. J.; Pitts, J. N., Jr. *Chemistry of the Upper and Lower Atmosphere: Theory, Experiments, and Applications*; 1st ed.; Academic Press: San Diego, CA, 1999.
(18) Kolb, C. E.; Worsnop, D. R. *Annu. Rev. Phys. Chem.* **2012**, *63*, 471−491.
(19) Seinfeld, J. H.; Pandis, S. N. *Atmospheric Chemistry and Physics: From Air Pollution to Climate Change*; 2nd ed.; John Wiley and Sons, Inc.: Hoboken, NJ, 2006.
(20) In *Fourth Assessment Report of the Intergovernmental Panel on Climate Change, 2007*; Solomon, S., Qin, D., Manning, M., Chen, Z., Marquis, M., Averyt, K. B., Tignor, M., Miller, H. L., Eds.; Cambridge University Press: Cambridge, U.K., 2007.
(21) Donaldson, D. J.; Guest, J. A.; Goh, M. C. *J. Phys. Chem.* **1995**, *99*, 9313−9315.
(22) Kester, D. R.; Duedall, I. W.; Connors, D. N.; Pytkowicz, R. M. *Limnol. Oceanogr.* **1967**, *12*, 176−179.
(23) *CRC Handbook of Chemistry and Physics*, 92nd ed. [Online]; Haynes, W. M.; CRC Press: Boca Raton, FL, 2012.
(24) Chen, X. K.; Minofar, B.; Jungwirth, P.; Allen, H. C. *J. Phys. Chem. B* **2010**, *114*, 15546−15553.
(25) Schwartz, S. E. *Nature* **1988**, *336*, 441−445.
(26) Pye, C. C.; Rudolph, W. W. *J. Phys. Chem. A* **2001**, *105*, 905−912.
(27) Zhou, J.; Santambrogio, G.; Brümmer, M.; Moore, D. T.; Wöste, L.; Meijer, G.; Neumark, D. M.; Asmis, K. R. *J. Chem. Phys.* **2006**, *125*, 111102(1−4).
(28) Zhang, Y.-H.; Chan, C. K. *J. Phys. Chem. A* **2002**, *106*, 285−292.
(29) Roberts, J. M.; Osthoff, H. D.; Brown, S. S.; Ravishankara, A. R. *Science* **2008**, *321*, 1059.
(30) Claeys, M.; Wang, W.; Ion, A. C.; Kourtchev, I.; Gelencsér, A.; Maenhaut, W. *Atmos. Environ.* **2004**, *38*, 4093−4098.
(31) Boge, O.; Miao, Y.; Plewka, A.; Herrmann, H. *Atmos. Environ.* **2006**, *40*, 2501−2509.
(32) Auer, B. M.; Skinner, J. L. *J. Phys. Chem. B* **2009**, *113*, 4125−4130.
(33) Allen, H. C.; Casillas-Ituarte, N. N.; Sierra-Hernández, M. R.; Chen, X.; Tang, C. Y. *Phys. Chem. Chem. Phys.* **2009**, *11*, 5538−5549.
(34) Ishiyama, T.; Morita, A. *J. Phys. Chem. C* **2011**, *115*, 13704−13716.
(35) Kido Soule, M. C.; Blower, P. G.; Richmond, G. L. *J. Phys. Chem. A.* **2007**, *111*, 3349−3357.
(36) Mucha, M.; Frigato, T.; Levering, L. M.; Allen, H. C.; Tobias, D. J.; Dang, L. X.; Jungwirth, P. *J. Phys. Chem. B* **2005**, *109*, 7617−7623.
(37) Rao, Y.; Subir, M.; McArthur, E. A.; Turro, N. J.; Eisenthal, K. B. *Chem. Phys. Lett.* **2009**, *477*, 242−244.
(38) Pegram, L. M.; Record, M. T. *Proc. Natl. Acad. Sci. U.S.A.* **2006**, *103*, 14278−14281.
(39) Du, Q.; Superfine, R.; Freysz, E.; Shen, Y. R. *Phys. Rev. Lett.* **1993**, *70*, 2313−2316.
(40) Bianco, R.; Wang, S.; Hynes, J. T. *J. Phys. Chem. A* **2008**, *112*, 9467−9476.
(41) Zhang, Y.; Cremer, P. *Curr. Opin. Chem. Biol.* **2006**, *10*, 658−663.
(42) Stuart, S. J.; Berne, B. J. *J. Phys. Chem. A* **1999**, *103*, 10300−10307.
(43) Tian, C. S.; Byrnes, S. J.; Han, H. L.; Shen, Y. R. *J. Phys. Chem. Lett.* **2011**, *2*, 1946−1949.
(44) Tian, C. S.; Ja, N.; Waychunas, G. A.; Shen, Y. R. *J. Am. Chem. Soc.* **2008**, *130*, 13033−13039.
(45) Casillas-Ituarte, N. N.; Callahan, K. M.; Tang, C. Y.; Chen, X. K.; Roeselova, M.; Tobias, D. J.; Allen, H. C. *Proc. Natl. Acad. Sci. U.S.A.* **2010**, *107*, 6616−6621.
(46) Gopalakrishnan, S.; Jungwirth, P.; Tobias, D. J.; Allen, H. C. *J. Phys. Chem. B* **2005**, *109*, 8861−8872.
(47) Hua, W.; Jubb, A. M.; Allen, H. C. *J. Phys. Chem. Lett.* **2011**, *2*, 2515−2520.
(48) Nihonyanagi, S.; Ishiyama, T.; Lee, T.-K.; Yamaguchi, S.; Bonn, M.; Morita, A.; Tahara, T. *J. Am. Chem. Soc.* **2011**, *133*, 16875−16880.
(49) Feng, R.-R.; Bian, H.-T.; Guo, Y.; Wang, H.-F. *J. Chem. Phys.* **2009**, *130*, 134710(1−6).
(50) Stiopkin, I. V.; Weeraman, C.; Pieniazek, P. A.; Shalhout, F. Y.; Skinner, J. L.; Benderskii, A. V. *Nature* **2011**, *474*, 192−195.
(51) Xu, M.; Tang, C. Y.; Jubb, A. M.; Chen, X.; Allen, H. C. *J. Phys. Chem. C* **2009**, *113*, 2082−2087.
(52) Otten, D. E.; Onorato, R.; Michaels, R.; Goodknight, J.; Saykally, R. J. *Chem. Phys. Lett.* **2012**, *519*−*520*, 45−48.
(53) Miyamae, T.; Morita, A.; Ouchi, Y. *Phys. Chem. Chem. Phys.* **2008**, *10*, 1985−2124.
(54) Ishiyama, T.; Morita, A.; Miyamae, T. *Phys. Chem. Chem. Phys.* **2011**, *13*, 20965−20973.
(55) Boyd, R. W. *Nonlinear Optics*; Academic Press: San Diego, CA, 1992; Vol. *1*.
(56) Johnson, C. M.; Tyrode, E. *Phys. Chem. Chem. Phys.* **2005**, *7*, 2635−2640.
(57) Zhao, L.-J.; Zhang, Y.-H.; Wei, Z.-F.; Cheng, H.; Li, X.-H. *J. Phys. Chem. A* **2006**, *110*, 951−958.
(58) Callahan, K. M.; Casillas-Ituarte, N. N.; Xu, M.; Roeselová, M.; Allen, H. C.; Tobias, D. J. *J. Phys. Chem. A* **2010**, *114*, 8359−8368.
(59) Choe, Y.-K.; Tsuchida, E.; Ikeshoji, T. *J. Chem. Phys.* **2007**, *126*, 154510(1−9).
(60) Horn, A. B.; Sully, K. J. *Phys. Chem. Chem. Phys.* **1999**, *1*, 3801−3806.
(61) Knopf, D. A.; Luo, B. P.; Krieger, U. K.; Koop, T. *J. Phys. Chem. A* **2003**, *107*, 4322−4332.
(62) Re, S.; Osamura, Y.; Morokuma, K. *J. Phys. Chem. A* **1999**, *103*, 3535−3547.
(63) Vchirawongkwin, V.; Kritayakornupong, C.; Rode, B. M. *J. Phys. Chem. B* **2010**, *114*, 11561−11569.
(64) Walrafen, G. E.; Yang, W.-H.; Chu, Y. C. *J. Phys. Chem. A* **2002**, *106*, 10162−10173.
(65) Eigen, M.; Tamm, K. *Z. Elektrochem. Angew. Phys. Chem.* **1962**, *66*, 93−107.
(66) Akilan, C.; Rohman, N.; Hefter, G.; Buchner, R. *ChemPhysChem* **2006**, *7*, 2319−2330.
(67) Buchner, R.; Capewell, S. G.; Hefter, G.; May, P. M. *J. Phys. Chem. B* **1999**, *103*, 1185−1192.
(68) Chaban, G. M.; Huo, W. M.; Lee, T. J. *J. Chem. Phys.* **2002**, *117*, 2532−2537.
(69) Daly, F. P.; Brown, C. W.; Kester, D. R. *J. Phys. Chem.* **1972**, *76*, 3664−3668.
(70) Dong, J.-L.; Li, X.-H.; Zhao, L.-J.; Xiao, H.-S.; Wang, F.; Guo, X.; Zhang, Y.-H. *J. Phys. Chem. B* **2007**, *111*, 12170−12176.
(71) Fung, K. H.; Tang, I. N. *Appl. Opt.* **1992**, *27*, 206−208.
(72) Guo, X.; Shou, J.; Zhang, Y.; Reid, J. P. *Analyst* **2010**, *135*, 495−502.
(73) Klassen, B.; Aroca, R.; Nazri, G. A. *J. Phys. Chem.* **1996**, *100*, 9334−9338.
(74) Marcus, Y.; Hefter, G. *Chem. Rev.* **2006**, *106*, 4585−4621.
(75) Nucci, N. V.; Vanderkooi, J. M. *J. Mol. Liq.* **2008**, *143*, 160−170.
(76) Pye, C. C.; Rudolph, W. W. *J. Phys. Chem. A* **1998**, *102*, 9933−9943.
(77) Rudolph, W.; Brooker, M. H.; Tremaine, P. R. *J. Solution Chem.* **1997**, *26*, 757−777.
(78) Rudolph, W. W.; Brooker, M. H.; Tremaine, P. R. *J. Solution Chem.* **1999**, *28*, 621−630.
(79) Rudolph, W. W.; Irmer, G.; Hefter, G. T. *Phys. Chem. Chem. Phys.* **2003**, *5*, 5253−5261.
(80) Vollmar, P. M. *J. Chem. Phys.* **1963**, *39*, 2236−2248.
(81) Wachter, W.; Fernandez, S.; Buchner, R.; Hefter, G. *J. Phys. Chem. B* **2007**, *111*, 9010−9017.
(82) Xu, M.; Larentzos, J. P.; Roshdy, M.; Criscenti, L. J.; Allen, H. C. *Phys. Chem. Chem. Phys.* **2008**, *10*, 4793−4801.
(83) Wang, F.; Zhang, Y.-H.; Li, S.-H.; Wang, L.-Y.; Zhao, L.-J. *Anal. Chem.* **2005**, *77*, 7148−7155.
(84) Watanabe, D.; Hamaguchi, H. *J. Chem. Phys.* **2005**, *123*, 034508(1−7).

(85) Zhang, H.; Wang, S.; Sun, C.-C. *J. Chem. Phys.* **2011**, *135*, 084309(1−10).
(86) Zhang, H.; Zhang, Y.-H.; Wang, F. *J. Comput. Chem.* **2008**, *30*, 493−503.
(87) Zhang, Y.-H.; Chan, C. K. *J. Phys. Chem. A* **2000**, *104*, 9191−9196.
(88) Schroder, D.; Duchachkova, L.; Tarabek, J.; Karwowska, M.; Fijalkowski, K. J.; Oncak, M.; Slavicek, P. *J. Am. Chem. Soc.* **2011**, *113*, 2444−2451.
(89) Berenblut, B. J.; Dawson, P.; Wilkinson, G. R. *Spectrochim. Acta, Part A* **1973**, *29A*, 29−36.
(90) Ma, G.; Allen, H. C. *Langmuir* **2006**, *22*, 5341−5349.
(91) Bock, C. W.; Markham, G. D.; Katz, A. K.; Glusker, J. P. *Theor. Chem. Acc.* **2006**, *115*, 100−112.
(92) Yacovitch, T. I.; Wende, T.; Jiang, L.; Heine, N.; Meijer, G.; Neumark, D. M.; Asmis, K. R. *J. Phys. Chem. Lett.* **2011**, *2*, 2135−2140.